

Length of standing jumps along granular flows down smooth inclines

Ségolène Méjean ^{*}

*University Grenoble-Alpes, Irstea, UR ETGR, F-38402 St-Martin-d'Hères, France
and School of Civil Engineering, The University of Sydney, Sydney NSW 2006, Australia*

François Guillard

School of Civil Engineering, The University of Sydney, Sydney NSW 2006, Australia

Thierry Faug[†]

University Grenoble-Alpes, Irstea, UR ETGR, F-38402 St-Martin-d'Hères, France

Itai Einav

School of Civil Engineering, The University of Sydney, Sydney NSW 2006, Australia



(Received 13 September 2018; accepted 11 February 2020;
published 13 March 2020)

Granular jumps—the change in height and depth-averaged velocity during granular flows—occur during transitions from thin and fast flows (supercritical) to thick and slow flows (subcritical). The present paper describes discrete element method simulations inspired by recent laboratory experiments, which produce standing jumps in two-dimensional free-surface dry granular flows down a slope. Special attention is paid to characterizing and measuring the finite length of those standing granular jumps, as well as to deciphering their internal structure. By varying macroscopic quantities, such as slope angle and mass discharge, and microscopic properties, such as interparticle friction and grain diameter, a rich variety of granular jump patterns is observed. Hydraulic-like granular jumps with an internal waterlike roller are identified, in addition to diffuse laminar granular jumps and steep colliding granular jumps. Moreover, a recently established depth-averaged relation for the prediction of jump heights is fed with the measured jump length and fitted against the numerical simulations to examine the effective friction in the granular medium for each type of jump. The dominant component of the general friction law is found to be different when transitioning from one jump pattern to the others. This study demonstrates that the granular jump pattern, and particularly its geometry and internal structure, can offer a stringent test for addressing the dissipation mechanisms that govern the flowability of granular media.

DOI: [10.1103/PhysRevFluids.5.034303](https://doi.org/10.1103/PhysRevFluids.5.034303)

I. INTRODUCTION

Granular materials are ubiquitous in nature and are often involved in a myriad of industrial processes. When an assembly of grains experiences different boundary conditions, it can move across different states of matter from solid through to liquid and gaseous phases [1,2]. Those transitions are for instance observed in free-surface flows of dry granular materials down a slope

^{*}segolene.mejean@irstea.fr

[†]thierry.faug@irstea.fr

[3], which are relevant to a number of large-scale mass flows in nature, such as landslides, debris flows, and snow avalanches. When the front of a granular flow hits a solid surface, either horizontal [4] or inclined [5], its profile presents a sudden change in height and velocity. As granular flows impact barriers—which are commonly used for stopping or diverting landslides, debris flows, and avalanches—they experience such a sudden change in height and velocity, as reported in Refs. [6–8] and references therein. The profile change in height and velocity is called a *granular jump* by analogy to hydraulic jumps [9–11]. Propagating granular jump patterns also form at the transition between steady and unsteady flows, in granular heap flows when adding a small amount of water to monodisperse glass beads [12] or during spreading and deposition of a granular mass upon passing from a confined inclined chute to a horizontal run out zone [13]. Granular jumps can be gradual or very sharp and accompanied by a change in density when the incoming flow is dilute enough (far below the random close packing density of a quasistatic assembly of grains). Granular jumps along free-surface flows are often described by classical shallow-water shock equations, which are based on the simplification that the jump volume shrinks into a singular surface [9,14]. However, granular jumps do have a finite volume (and length), as earlier stated by Savage [15] and clearly demonstrated from the laboratory study on standing jumps recently conducted by Faug *et al.* [16].

The overarching aim of the present study is to carefully analyze the properties that control the length of standing granular jumps, using the numerical discrete element method. The length of the standing granular jumps represents the efficiency of the material to dissipate energy as it transitions from a thin and fast flow to a thicker and slower flow. Therefore studying the length and internal structure of standing granular jumps can help in deciphering the various mechanisms at the origin of energy dissipation and thus advance the knowledge of the physics of dense granular flows. A recent study [18] proposed a general relation for the height ratio of a standing granular jump, h_*/h , as a function of the incoming Froude number of the flow $\text{Fr} = \bar{u}/(gh \cos \zeta)^{1/2}$, the normalized length of the jump, L/h , and the difference between the tangent of the slope angle ($\tan \zeta$) and the effective friction μ_e under a generalized Coulomb friction assumption (within the depth-averaged framework):

$$\frac{h_*}{h} = 2\sqrt{\frac{p}{3}} \cos \left[\frac{1}{3} \arccos \left(-\frac{q}{2} \sqrt{\frac{27}{p^3}} \right) \right] + \frac{1}{3} \frac{L}{h} \frac{K_0}{k_*} (\tan \zeta - \mu_e), \quad (1)$$

where p and q are given by the following expressions:

$$p = \frac{1}{k_* \frac{\rho_*}{\rho}} \left[2\beta \text{Fr}^2 + k + K_0 \frac{L}{h} (\tan \zeta - \mu_e) \right] + \frac{1}{3} \left[\frac{L}{h} \frac{K_0}{k_*} (\tan \zeta - \mu_e) \right]^2, \quad (2)$$

$$q = \frac{2\beta_* \text{Fr}^2}{k_* \left(\frac{\rho_*}{\rho} \right)^2} - \frac{2}{27} \left[\frac{L}{h} \frac{K_0}{k_*} (\tan \zeta - \mu_e) \right]^3 - \frac{1}{3} \frac{L}{h} \frac{K_0}{k_*} (\tan \zeta - \mu_e) \left[2\beta \text{Fr}^2 + k + K_0 \frac{L}{h} (\tan \zeta - \mu_e) \right]. \quad (3)$$

In the equations above, h is the thickness of the fast and thin incoming flow, \bar{u} the depth-averaged velocity, h_* the jump height (outgoing section of the jump), L the length of the jump, and g the gravity acceleration ($g = 9.81 \text{ m s}^{-2}$). $\rho = \phi \rho_P$ and $\rho_* = \phi_* \rho_P$ are the density of the granular bulk before and after the jump, respectively, where ϕ is the volume fraction and ρ_P is the grain material density (with the subscript $*$ for the region after the jump). The coefficient β refers to the shape of the velocity profile before the jump and is defined by $\bar{u}^2 = \beta \bar{u}^2$. The coefficients k and k_* account for the possible normal stress differences before and after the jump, respectively. For more details on this equation and related input parameters readers are referred to Ref. [18].

A recent experimental work [16] showed that considering a constitutive law based on the $\mu(I)$ rheology (see, for instance, Refs. [3,19,20]) through the effective friction μ_e defined above could give a good prediction of the jump height ratio h_*/h , provided that the incoming flows were steady and uniform. However, it is necessary to include an additional dissipative term, which depends on

the velocity-squared of the incoming flows, when the flows are fast and accelerating [18]. Moreover, no theoretical framework currently exists to predict the length of the jumps, thus rendering Eq. (1) not fully predictive. The present paper provides a detailed study of the internal structure of standing granular jumps and their length with the help of discrete element simulations in two dimensions. Several characterization methods based on the free surface of the jump, the velocity field, and the density field across the jump are proposed and compared. The influence of both macroscopic (mass discharge, slope angle) and microscopic (interparticle friction, grain diameter, restitution coefficient) input parameters on the length of the jumps are analyzed. The internal flow of the granular jumps allows us to clearly identify three different types of jumps, thus providing crucial information on the jump length variation. Moreover, by feeding Eq. (1) with the different measured jump lengths for each granular jump pattern identified, different variations of the effective friction with incoming flow conditions are derived. This demonstrates that the standing granular jump and particularly its length can be seen as a gauge for addressing more general physical insights into the rheology of granular flows.

Section II presents the numerical setup of the discrete element simulations used to produce the two-dimensional standing jumps, largely inspired by a laboratory device designed by Faug *et al.* [16]. Section III discusses the rich variety of granular jumps observed in the numerical simulations, confirming and further extending some of the results obtained with the previous laboratory tests [16]. In particular, a new type of granular jump is identified. Some more quantitative aspects associated with each type of granular jump are addressed in Sec. III. The variation of the jump length with both macroscopic and microscopic input parameters is analyzed in detail in Sec. IV for the different types of jump. Then Eq. (1) is applied to different types of granular jumps, allowing us to reveal different components controlling the structure of the friction law (effective friction in a depth-averaged framework) as a function of the incoming flow conditions (Sec. V). Finally, the paper ends with a discussion on the main outcomes of the present study and recommendation for future work (Sec. VI).

II. METHODS

A. Numerical set-up to produce standing jumps

Simulations using the discrete element method (DEM) are carried out with the YADE open source software [21], with spherical grains whose interaction is modeled by a viscoelastic force for normal contact directions and an elastic force capped by a Coulomb friction threshold for tangential contact directions. The details of this classical contact model used in DEM for dense granular flows are described in Ref. [22]. The stiffness coefficients are calculated from the values of the Young's modulus E , which was taken equal to 1×10^6 with respect to the limit of rigid grains condition and Poisson's coefficient ν taken equal to 0.3. The friction coefficient between moving grains and the bottom is $\mu_b = 0.25$. The grain density is $\rho_p = 2500 \text{ kg m}^{-3}$ to mimic the typical density of glass beads often used in laboratory experiments. The time step is $dt = 3 \times 10^{-4} \text{ s}$. The simulations are carried out in two dimensions, meaning that there is only one grain across the width of the flume and that side-walls effects are ignored, in contrast to the laboratory tests on granular jumps conducted in Ref. [16]. The grain diameter distribution varies 15% around the average diameter. This corresponds to a polydispersity which is high enough to avoid crystallization effects yet low enough to prevent grain segregation processes. Other important values of the model which have been varied for this study are presented in Table I.

The numerical setup used to produce the jumps is shown in Fig. 1, which describes an inclined plane of slope ζ that sustains a granular flow supplied by an upstream reservoir with an opening height H that is permanently feeding in grains. An initially closed retaining gate is placed at the exit of the incline. Under these conditions, a propagating granular jump is formed once the grains impact the retaining gate at the bottom of the plane. When the traveling jump reaches the middle of the incline, the retaining gate is moved vertically in order to make the jumps stationary. To this purpose, the incoming and outgoing discharge rates are continuously measured, while the retaining

TABLE I. The default and range of values for the parameters of the jumps: Height of the opening of the reservoir H , slope of the flume ζ , average grain diameter d , interparticle friction coefficient μ , friction coefficient between the grains and the bottom of the inclined plane μ_b , and the restitution coefficient between grains e .

	H (m)	ζ (deg)	d (m)	μ	μ_b	e
Default value	0.5	20	0.04	0.5	0.25	0.5
Range	0.4–1.1	22–50	0.02–0.06	0.04–1.0	–	0.1–1.0

gate is constantly adjusted vertically to balance the two flow rates. When the steady flow state is reached, the gate still has the possibility to move up or down if the outgoing discharge becomes different from the incoming discharge in order to maintain a steady flow during all the simulation. A number of numerical simulations are performed by varying the slope of the incline ζ and the opening height of the reservoir H (which controls the mass discharge). The effects of microscopic grain properties are also examined by varying the grain diameter d , the interparticle friction μ , and the restitution coefficient e .

B. From micro to macro: Coarse-graining

The spatial fields of volume fraction and velocity are calculated on a grid with a space-step of half a grain diameter d , using a coarse-graining method similar to the one described in Refs. [23–25]. The flowing particles are labeled from 1 to N . From statistical mechanics, the density of the granular medium at a given position \mathbf{r} and time t is defined by:

$$\rho(\mathbf{r}, t) = \sum_{\|\mathbf{r}_j - \mathbf{r}_i(t)\| \leq c} m_i \mathcal{W}(\|\mathbf{r} - \mathbf{r}_i(t)\|), \quad (4)$$

with $\|\mathbf{r} - \mathbf{r}_i\|$ the distance between the center of the i th grain with mass m_i to the point \mathbf{r} on the grid. A Lucy function \mathcal{W} was used as the coarse-graining kernel [26], which for two spatial dimensions

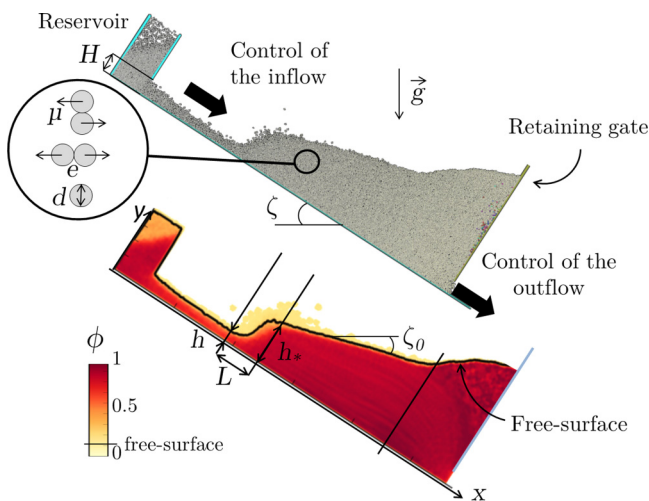


FIG. 1. Discrete element method numerical setup (top) and example of a volume fraction field obtained by coarse-graining (bottom).

takes the form [27,28]:

$$\mathcal{W}(r) = \begin{cases} \frac{5}{\pi c^2} \left[-3\left(\frac{r}{c}\right)^4 + 8\left(\frac{r}{c}\right)^3 - 6\left(\frac{r}{c}\right)^2 + 1 \right] & \text{if } r < c \\ 0 & \text{otherwise} \end{cases}. \quad (5)$$

The range of the Lucy function is here taken equal to $c = 2.5d$. The choice of this range is a compromise between a value large enough to smoothen out the discrete nature of the granular system and small enough to still observe the continuum gradients. From the literature, $c \gtrsim 2d$ is very often encountered. The sensitivity of the results to the coarse-graining width for the granular flow and jump problem investigated here was checked and is briefly discussed in Appendix A.

The coarse-grained velocity values $v(\mathbf{r}, t)$ are calculated from:

$$v(\mathbf{r}, t) = \frac{\sum_{\|\mathbf{r}_j - \mathbf{r}_i(t)\| \leq c} v(\mathbf{r}_i, t) m_i \mathcal{W}(\|\mathbf{r} - \mathbf{r}_i(t)\|)}{\rho_j(t)}. \quad (6)$$

When the steady state is reached, the coarse-grained fields are extracted every 1000 time steps (0.3 s) and averaged, such that the results is insensitive to increasing number of frames. The reader can refer to the end of Appendix A for a brief discussion on the choice made for time averaging of the data. The free surface is defined from the field of volume fraction ϕ , with a threshold of 0.15, which largely indicates a transition from a loose gaseouslike to a denser fluidlike medium. A typical result obtained for the volume fraction field is shown on Fig. 1. Furthermore, in the following the depth-averaged variables will also be described along the x axis of the inclined plane by averaging the values of the points of the grid that are under the free surface for each x , and weighting them by the density at that point, with f representing either the density ρ or the velocity v :

$$f(x) = \frac{\sum_{y \leq h(x)} \rho(x, y) f(x, y)}{\sum_{y \leq h(x)} \rho(x, y)}. \quad (7)$$

Some examples of the velocity profiles at different given positions along the chute extracted from the two-dimensional velocity field will be shown in Sec. III.

C. Defining the length(s) of the jump

The aim of the DEM simulations presented in the current paper is to define and determine accurately the length of standing granular jumps, as a closure relationship for Eq. (1). Until now, the jump length has always been defined only visually through observation of the free surface [16,18,22]. This definition is tacitly based on the assumption that the jump begins when the free surface is no longer parallel to the bottom and ends when it reaches a constant angle which corresponds to the minimum angle to have a flow. As can be seen in Fig. 2, a jump is characterized by a rapid change not only in the flow thickness h but also in the depth-averaged velocity \bar{u} and in the volume fraction ϕ . By considering h , \bar{u} , or ϕ , it is possible to define at least three different lengths for the jump.

The volume fraction was already used above as a criterion for determining the free surface of the flowing medium, i.e., to distinguish between the dense flowing layer and the gaseous phase of particles undergoing binary collisions above the free surface (viz., using the threshold of 0.15 in volume fraction on Fig. 1). However, Fig. 2 shows that the depth-averaged variation of the volume fraction along the x coordinate is not very smooth, so a criterion for defining the jump length based on volume fraction is probably not going to be reliable. That said, the length of the jump defined by the volume fraction appears to be very close to the length of the jump defined by the velocity.

Both the free-surface curve used in the previous studies [16,22] and the depth-averaged velocity curve proposed in the present study exhibit a smooth signal. Their corresponding curves also show the transition between the fast and thin flow regime (supercritical) and the slow and thick flow regime (subcritical). The start of the jump is relatively easy to determine. In the case of the velocity curve, this point is well defined in terms of the local maximum of the curve. In the case of the

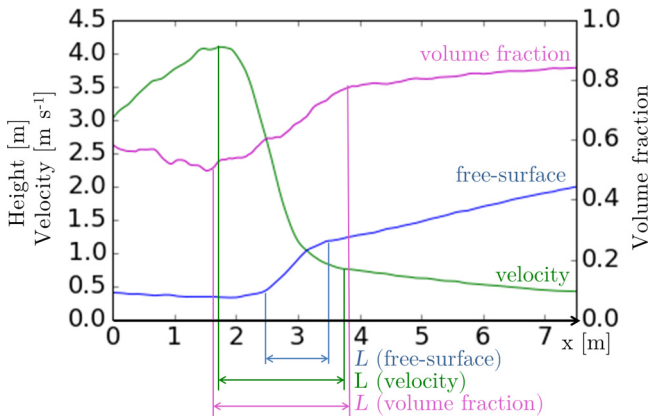


FIG. 2. Three different jump lengths identified for a single standing (laminar) granular jump, based on the depth-averaged variable considered: h (blue line), \bar{u} (green line), or ϕ (pink line). This jump was obtained with $\zeta = 28^\circ$, $H = 0.5$ m, $\mu = 0.5$, $d = 4.0$ cm.

free-surface curve, that point is well defined, too, as already discussed previously. The end of the jump is not as straightforward to determine, regardless of the criterion used (either the free surface or the depth-averaged velocity curves). However, in both cases, one can find the point where the curve describing the corresponding variable (h or \bar{u}) along the plane becomes a straight line. This method requires a smoothing of the function that describes the variable considered. The smoothing function used was a Savitzky-Golay filter [29], as it gave sufficiently smooth results without losing the information of the points where there are strong variations. Then the transition point is defined when the derivative of the function describing the variable becomes constant. As the two methods give different results, the question is then which of these two length definitions is the more relevant?

The length of the jump region can be considered as the length of a transition zone between two different possible stable flow states. That length should be a function of the given set of initial conditions (slope angle, discharge rate, frictional properties of the side and bottom walls, and the properties of the grains): Any disturbance from a stable state observed along the inclined plane should be considered as being a part of the jump region itself. Figure 2 shows that a disturbance already occurs on the depth-averaged velocity curve and the depth-averaged volume fraction curve while the changes are not yet detected on the free-surface curve. Moreover, the end of the jump given by the velocity curve (similarly to the one given by the volume fraction curve) stands beyond the end of the jump given by the free-surface curve (Fig. 2), suggesting that disturbances also occur after the end of the jump detected from the free-surface curve. For these reasons it seems reasonable to choose the depth-averaged velocity as the criterion to determine the jump region. In the rest of this study, the length L will always refer to the length of the jump measured from the velocity profile, as described above.

III. THE DIFFERENT TYPES OF JUMP

The numerical setup allows us to obtain a wide spectrum of standing granular jump patterns by varying the control parameters over the ranges listed in Table I. The restitution coefficient e between the grains did not have any discernible influence on the jumps created. For that reason, all the jumps reported in the present work are based on a restitution coefficient $e = 0.5$.

Figure 3(a) shows some examples of the streamlines inside the jumps obtained by coarse-graining the velocities from the DEM. A transition from steep jumps at high slope angles to much more diffuse jumps at the lower slope angles is observed. Under high mass discharges, the granular media tend to remain dense and nearly incompressible. In contrast, the jumps become much

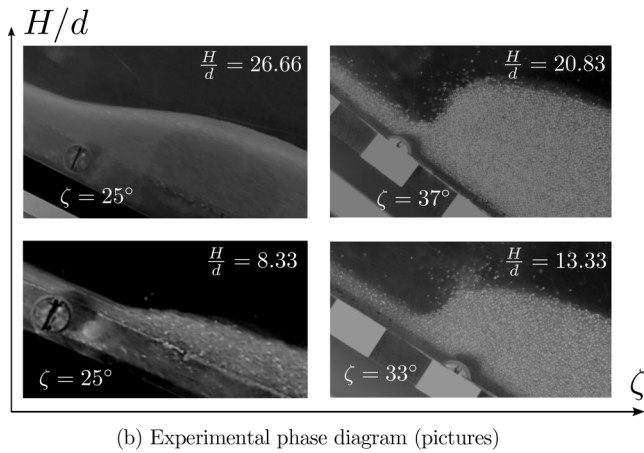
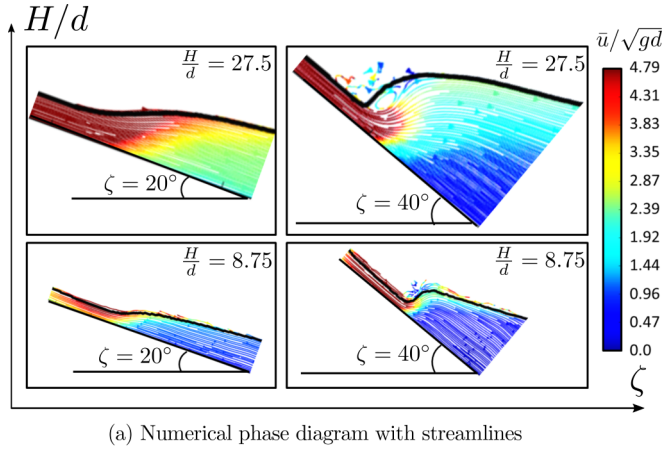


FIG. 3. Numerical and experimental phase diagrams of jump patterns for various slopes ζ and discharge height ratio H/d . (a) Phase diagram obtained numerically in the present study. The streamlines inside the jumps are drawn with a color indicating the local velocity. All the simulation use an interparticle friction $\mu = 0.5$ and a bottom friction $\mu_b = 0.25$. (b) Phase diagram obtained experimentally in Ref. [16] using glass beads.

more compressible at lower mass discharges. A recirculation zone can be identified under some specific conditions when either the slope angle and/or the mass discharge are high. Those different two-dimensional (2D) numerical jump patterns are fully consistent with previous 3D experimental results. Additionally, Fig. 3(b) shows the experimental phase diagram obtained in Ref. [16], which compares qualitatively well with the phase diagram obtained numerically [Fig. 3(a)] in the present study by varying both ζ and H . A quantitative comparison is not possible between the numerical simulations carried out in two dimensions and the laboratory tests, which were three dimensional, mostly because of the difference in 2D and 3D packing fractions.

The advantage of the current numerical simulations is that the streamlines can be accessed before, inside, and after the jumps. Recirculation zones can for instance be clearly identified in the top right corner of the numerical phase diagram in Fig. 3(a), with one of the streamlines showing a rolling pattern that is developing at the foot of the steep jump. A criterion to identify the recirculation more easily than with the streamlines (and even estimate its size) will be discussed in Sec. III B.

Recirculation patterns are also observed once the interparticle friction μ is decreased to values smaller than a critical friction μ_{cr} , as depicted on Fig. 4. The recirculation here always takes

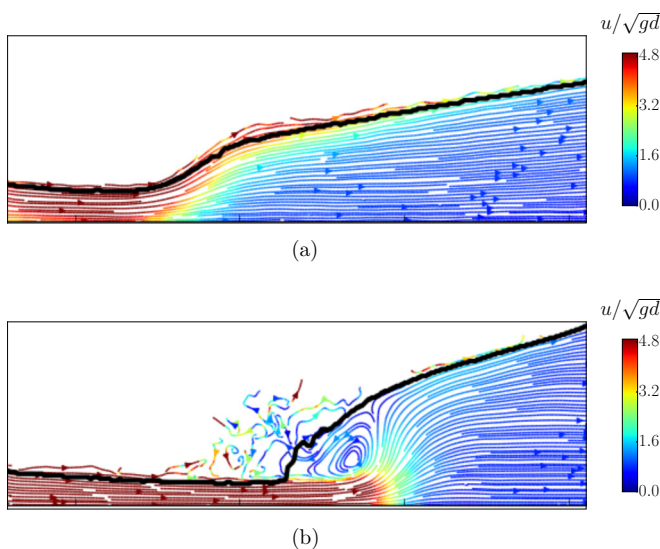


FIG. 4. Transition from (a) a laminar granular jump ($\mu = 0.8 > \mu_{\text{cr}}$) to (b) a hydraulic-like granular jump with the presence of a waterlike roller ($\mu = 0.1 < \mu_{\text{cr}}$). The streamlines are drawn in each jump as in Fig. 3(a) with colors representing the corresponding velocity.

place into the interior of the jump and can run along almost the entire length of the jump. This type of recirculation is different from the one observed in the phase diagram [Fig. 3(a)], which is located close to the free surface at the foot of the jump. Note that the recirculation observed in the phase diagram at high slope angles is either just below the free surface (high discharge rates) or above (lower discharge rates). The recirculation pattern observed under small values of interparticle friction is closer to the fully developed internal roller that one observes with hydraulic (nonfrictional) flows. Such waterlike granular rollers were not observed in the experimental work in Ref. [16], as the interparticle friction coefficient is inherent to the material and thus cannot be easily controlled experimentally. It is worthwhile to note that in our DEM simulations we did not observe any transition between one jump pattern to another while keeping the micro and macro parameters constant, unlike previous experimental studies that found multiple solutions for the same set of parameters for different geometrical configurations. For instance, Viroulet *et al.* [8] recently studied granular flows over a smooth bumplike obstacle and highlighted the existence of two solutions—either a detached jet downstream or a granular jump upstream, depending on whether or not some grains at rest were initially settled in front of the bump before the impact of the incoming granular stream. Also, Gray and Cui [30] were able to produce strong oblique shocks instead of weak shocks by carefully controlling the downstream boundary conditions in their tests on deflected granular flows (both the strong and weak oblique shocks being predicted by their theory). In the following, we will discuss in more detail the properties of the different types of stable jump patterns observed in our simulations.

A. Laminar granular jumps

Figure 2 shows the height of the free surface, the depth-averaged velocity, and the depth-averaged volume fraction of a laminar granular jump. The streamlines of this type of jump [see the two pictures on the left side of Fig. 3(a)] are showing a smooth transition from one stable state (thin flow, high velocity) to another (thick flow, low velocity).

In this kind of jumps, the energy is deemed to dissipate due to the friction developing between the grains. The depth-averaged volume fraction in such jumps (see purple curve in Fig. 2) exhibits a

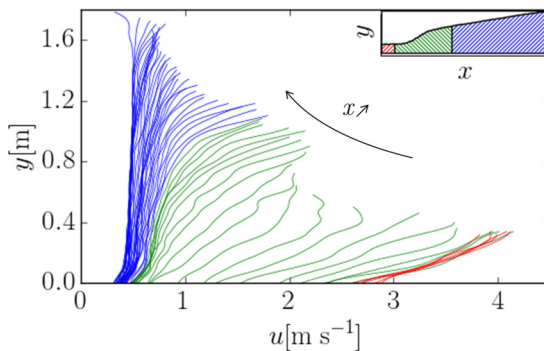


FIG. 5. Velocity profiles of a laminar granular jump ($\zeta = 24^\circ$, $d = 4$ cm, $H = 0.5$ m, $\mu = 0.5$) before (red), inside (green), and after (blue) the jump. The velocity profiles shown were measured every 0.12 m along the inclined plane.

monotonic growth while transitioning from one state to the other. We will show in Sec. IV that, for such laminar granular jumps, the length L of the jump could be expressed as a linear function of the incoming thickness h .

Figure 5 shows the velocity profiles of a laminar jump. As discussed in previous studies about granular flows down smooth inclines [16,31], the incoming velocity profile (red curves in Fig. 5) follows a Bagnold profile with a sliding velocity at the bottom. The velocity as a function of depth $u(y)$ is given by:

$$u(y) = u_b(\zeta) + A(\zeta)\sqrt{gd} \left[\left(\frac{h - y_0}{d} \right)^{3/2} - \left(\frac{h - y_0}{d} - \frac{y - y_0}{d} \right)^{3/2} \right], \quad (8)$$

with $u_b(\zeta)$ the sliding velocity and $A(\zeta)$ a coefficient, both dependent on the slope angle ζ , and $y_0 = 1.5d$ the typical thickness of the layer made of grains sliding on the chute bottom (roughly assumed to be independent on ζ). Empirical expressions for $u_b(\zeta)$ and $A(\zeta)$ are discussed in Ref. [16].

After the end of the jump (blue curves in Fig. 5), the velocity profile is totally different: The sliding velocity is much lower and the shear rates are much weaker. Inside the jump region (green curves in Fig. 5), the velocity profiles adjust from the upstream stable flow state to the downstream gradually decelerating flow state. The curves showing those profiles are well separated because of a significant decrease of velocity along the x axis within the jump region, while they collapse well before the jump (nonaccelerating flow) and are quite close to each other after the jump (slightly decelerating flow).

B. Steep colliding granular jumps

Starting from the conditions under which a laminar granular jump is formed, increased slope angle as in Fig. 6 gradually destabilizes the jump, with the possibility of an accompanying recirculation pattern. The jump region in that case is very short and steep, while the gravity forces are having a strong influence on the flow. In particular, the grains of the incoming collisional flow add a strong eroding force on the grains inside the jump, whereas the grains on top of the jump are pulled down by gravity in an avalanching process. This process seems to correspond to the recirculation eddy at the foot of granular jumps previously reported by Brennen *et al.* [9] and Gray *et al.* [14] in their experiments at high Froude numbers.

This recirculation can be seen in the streamlines [see the pictures depicted on the first row of Fig. 6 for cases (c), (d), and (e)]. This phenomenon becomes even more obvious when plotting the variations of the depth-averaged volume fraction $\phi(x)$ along the chute as displayed on Fig. 6 (second row). Here a significant drop in volume fraction takes place from the middle to the end of the jump

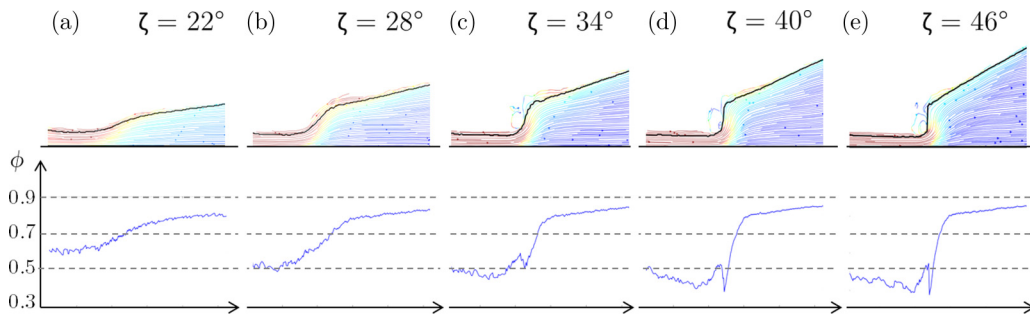


FIG. 6. Transition from a laminar granular jump [cases (a) and (b)] to a steep colliding granular jump [cases (c), (d), and (e)] by varying the slope: streamlines (first row) and longitudinal variation of the depth-averaged volume fraction (second row).

for cases (c), (d) and (e). The general profile resembles that of a laminar granular jump but the presence of the significant drop in volume fraction emphasises the granular recirculation process.

Figure 7 shows the velocity profiles of a steep (recirculating) colliding jump. As for the laminar granular jumps, the incoming velocity profiles (red curves in Fig. 7) follow a Bagnold profile with a sliding velocity [Eq. (8)]. The velocity profiles after the jump (blue curves in Fig. 7) are also similar to the velocity profiles after a laminar granular jump (blue curves in Fig. 5). However, because of the recirculation, the velocity profiles inside a steep colliding granular jump (green curves in Fig. 7) are very different from the ones in a laminar granular jump (green curves in Fig. 5). At a given position x inside the jump, the magnitude of the velocity is first increasing with the height, and then strongly decreases beyond a certain position y . At some points, the decrease is so strong that the velocity along the inclined plane may even become negative, clearly indicating a recirculation process. At the same time, the sliding velocity is decreasing rapidly. Close to the end of the jump, the upper part of the velocity profile is increasing again, in a way that aligns with the outgoing flow after the jump.

C. Hydraulic-like granular jumps with an internal roller

The hydraulic-like jump is characterized by a waterlike roller developing within the jump, below the free surface of the flow [see Fig. 4(b)]. Its dynamics is different from the one of the colliding jump with granular recirculation developing close to the free surface, as discussed in the previous subsection. The hydraulic-like jump is created when the interparticle friction is lowered below a

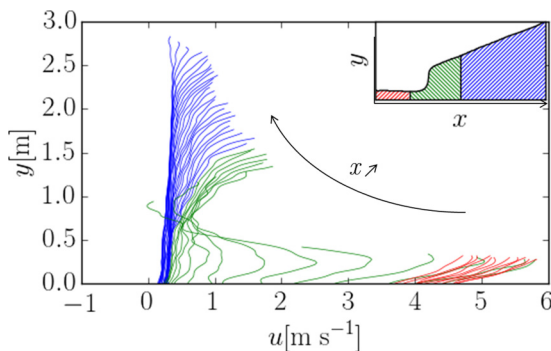


FIG. 7. Velocity profiles of a steep colliding granular jump ($\zeta = 38^\circ$, $d = 4$ cm, $H = 0.5$ m, $\mu = 0.5$) before (blue), inside (green), and after (red) the jump. The velocity profiles shown were measured every 0.12 m along the inclined plane.

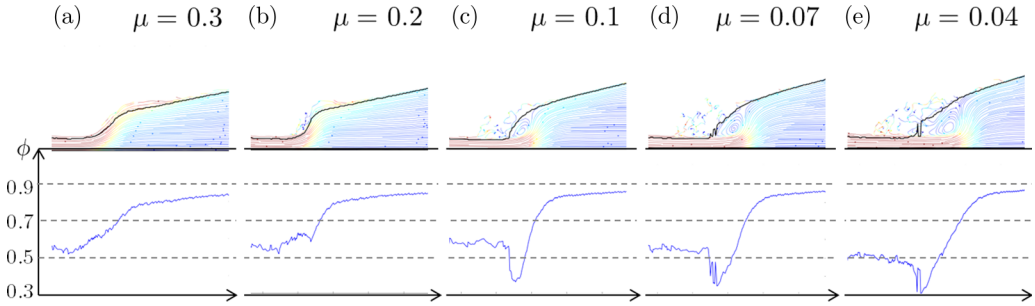


FIG. 8. Transition from a laminar granular jump (a) to a hydraulic-like granular jump with a waterlike roller [(b), (c), (d), and (e)] by varying the interparticle friction coefficient: Streamlines (first row) and longitudinal variation of the depth-averaged volume fraction (second row).

critical friction coefficient μ_{cr} . As the interparticle friction decreases, the properties of the flow inside the jump tend to be similar to what is commonly observed for a frictionless fluid like water. The instable zone of the recirculation looks like the roller phenomenon known to appear in hydraulic jumps (see Ref. [18] and references therein). Like rollers in hydraulic jumps in water, this large recirculation zone seems to have a strong influence on the other features of the jump.

Figure 8 shows the transition from a laminar granular jump to an hydraulic-like jump with a presence of an internal waterlike roller, in terms of the streamlines and the depth-averaged volume fraction. The waterlike roller may extend along almost the entire length of the jump. The drop in volume fraction identifying the recirculation zone does not appear in the middle of the jump like for the colliding granular jumps described in the previous section, but at the very beginning, and it is wider, thus indicating a different leading mechanism at stake. This difference can also be seen by comparing the velocity fields shown by the color of the streamlines depicted on Fig. 6 and Fig. 8. In the first case [cases (c), (d), and (e) in Fig. 6], the rapid incoming flow stays attached to the free surface and the recirculation takes place above the free surface, while it penetrates far into the jump in the second case [cases (c), (d), and (e) in Fig. 8], when the friction between the grains is very low, thus offering much less resistance to the incoming stream.

Figure 9 shows the velocity profiles of a hydraulic-like jump. Because of the low friction between the grains, the velocity profiles are very different from those in laminar granular jumps (Fig. 5) and colliding jumps with recirculation (Fig. 7). The incoming velocity profiles do not follow a Bagnold profile anymore, as can be seen from the red curves drawn in Fig. 9. The incoming flows look like

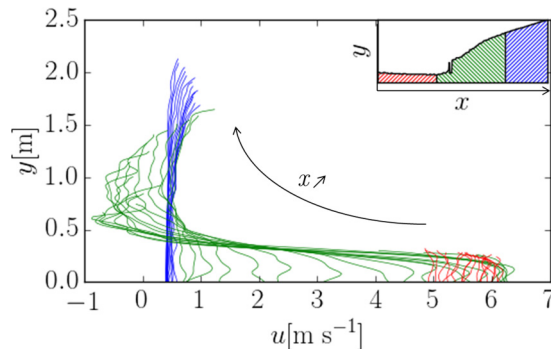


FIG. 9. Velocity profiles of a hydraulic-like jump ($\zeta = 25^\circ$, $d = 4$ cm, $H = 0.5$ m, $\mu = 0.04$) before (red), inside (green), and after (blue) the jump. The velocity profiles shown were measured every 0.12 m along the inclined plane.

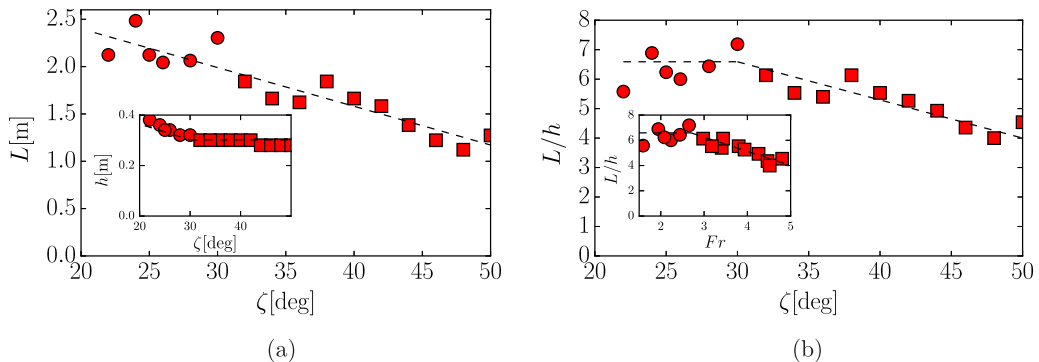


FIG. 10. Jump length L (a) and jump length relative to incoming flow thickness L/h (b) versus the slope angle ζ . Inset of (a): Incoming thickness of the flow h as a function of ζ . Inset of (b): Jump length relative to the incoming flow as a function of the Froude number. The circles correspond to the granular laminar jumps and the squares to the steep colliding granular jumps with recirculation.

a plug flow with nearly no shear over depth. After the jump (blue curves in Fig. 9), the profiles are more similarly to what we observe in both laminar and colliding granular jumps. This means that the friction between grains does not play such an important role after the jump. As those jumps are characterized by a roller, some velocity profiles inside the jump (green curves in Fig. 9) exhibit velocities that are sometimes largely negative. The overall shape of those velocity profiles inside the hydraulic-like jump with an internal waterlike roller differs from the shape of the profiles measured in the steep colliding jump with free-surface recirculation.

It is worthy to note that Figs. 5, 7, and 9 all indicate that the criterion based on the depth-averaged velocity defined in Sec. II C is accurate enough to delimitate the three zones before, inside, and after the jump.

IV. JUMP LENGTH VARIATION WITH INPUT PARAMETERS

In this section, a detailed investigation on the influence of different parameters on the jump patterns and the length of the jump (based on the depth-averaged velocity as discussed in Sec. II C) is presented. First, the effect of varying the slope angle, the mass discharge and the grain diameter for a given interparticle friction greater than the bottom friction is studied. Second, the effect of varying interparticle friction is analyzed.

A. Slope angle

The slope angle ζ , which controls the Froude number $Fr = \bar{u}/(gh \cos \zeta)^{1/2}$ of the incoming flow on a smooth bottom [16, 18], has a strong influence on the jump pattern: The diffuse jumps at small Fr become steeper with increasing Fr and a granular recirculation zone appears. That recirculation zone can be seen as the result of a stable granular flow (whose free surface is inclined at ζ_0) being eroded by the thin and fast incoming collisional flow, and thus producing backward avalanche flows starting from the top of the jump. The recirculation zone observed at high ζ ceases when the kinetic energy of the fast incoming collisional flow (and its high eroding capacity) is reduced at lower ζ .

The length of the jump is decreasing with the slope angle [see Fig. 10(a)]. When the jump is purely laminar, the incoming thickness of the flow h is also decreasing with the slope angle, proportionally to the jump length [see circles in the inset of Fig. 10(a)]. However, above a certain slope angle, the incoming thickness does not decrease any longer [squares in the inset of Fig. 10(a)]. The relative jump length L/h is therefore constant when the jump is purely laminar (L is a function which increases linearly with h) and starts decreasing with the slope angle (and thus the

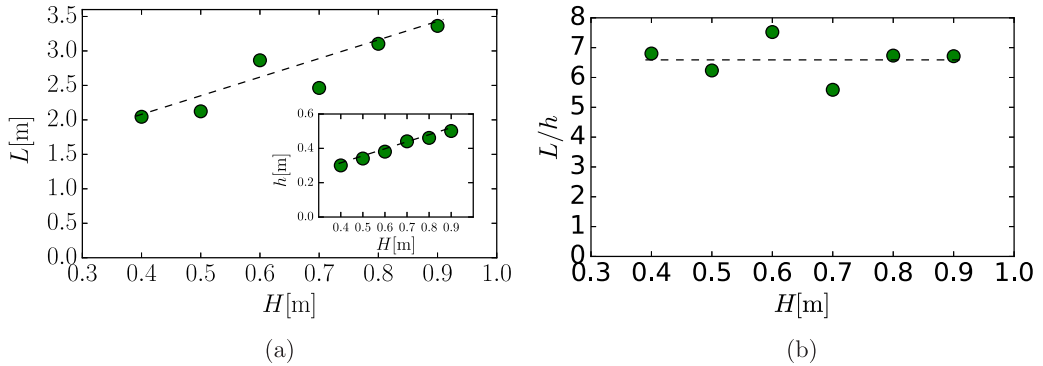


FIG. 11. Jump length L (a) and jump length relative to incoming flow thickness L/h (b) versus the opening height H at the exit of the tank (which controls the mass discharge). Inset in (a): Thickness h of the incoming flow as a function of the opening height H of the reservoir. Since L versus H and h versus H have the same slope in (a), L/h in (b) is independent of the mass discharge.

Froude number) when some recirculation appears, as shown in Fig. 10(b). This yields a decrease of L/h when Fr is increased [inset in Fig. 10(b)], in strong contrast with what would be observed in hydraulic flows (cf. the data gathered on Fig. 2(d) in Ref. [18] for water).

B. Mass discharge

The length of the jump is an increasing function of the opening height H of the gate at the exit of the tank, as shown in Fig. 11(a). Comparing Fig. 11(a) with the inset of Fig. 11(a), one observes that the increase of the jump length L with the opening height H , and the increase of the thickness h of the incoming flow with H are proportional [see black dashed lines in Fig. 11(a)]. Thus, normalizing the jump length by the thickness of the incoming flow leads to the result that L/h is essentially independent of the mass discharge [Fig. 11(b)]. In other words, the length L of the laminar granular jump is only a function of the incoming thickness h .

C. Grain diameter

Still considering laminar granular jumps, an increase in the grain diameter produces similar effects as the ones observed with an increase of the opening height of the reservoir. The increase of the length L of the jump with the grain diameter d is proportional to the increase of the thickness h of the incoming flow with d [see the black dashed lines in Fig. 12(a) and its inset]. Thus, L is a function of h only, and the normalized length L/h remains essentially constant with the grain diameter as depicted in Fig. 12(b).

D. Interparticle friction

The effect of varying the interparticle friction becomes significant once the interparticle friction falls below a critical friction μ_{cr} . For μ greater than μ_{cr} , the granular jump exhibits the smoothed streamlines, and the value of the interparticle friction does not have a strong influence on the jump length [see Fig. 13(a)]. For μ smaller than μ_{cr} , the curvature of the streamlines increases and a hydraulic-like roller forms inside the jump, which seems to influence the jump length [Fig. 13(a)]. However, the jump length relative to the thickness of the incoming flow remains nearly unchanged by varying μ .

To further highlight the transition from laminar granular jumps to hydraulic-like granular jumps (with the presence of a waterlike roller), the evolution of Fr , h_*/h , ζ_0 , and ϕ are drawn on Fig. 14. A sharp increase of h_*/h is observed when μ decreases below μ_{cr} , consistent with the simultaneous

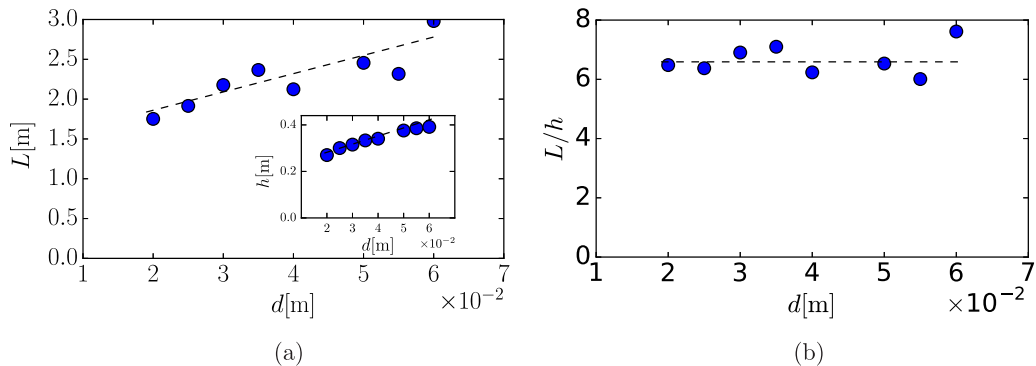


FIG. 12. (a) Jump length L , (b) jump length relative to incoming flow thickness L/h versus the grain diameter d . Inset in (a): Thickness h of the incoming flow as a function of d . L versus d and h versus d in (a) have the same slope, thus L/h in (b) is independent of d .

sharp increase of Fr , while ϕ remains nearly insensitive to μ . In addition, the angle ζ_0 at which the free surface of the superstable flow downstream of the jump is inclined drops and tends toward zero. This asymptotic behavior resembles the phenomenon observed with water flows.

V. DISCUSSION

A. Jump height ratio

Referring to Eq. (1) described in the introduction, Fig. 15 depicts the thickness of the jump h_* relative to the thickness of the incoming flow h as a function of the Froude number of the incoming flow for all jumps. The prediction of the Bélanger equation [32], classically used in hydraulics, suggests:

$$\frac{h_*}{h} = \frac{1}{2}(\sqrt{1 + Fr^2} - 1), \quad (9)$$

and is also plotted. This is, in a fact, a reduced form of Eq. (1) for $\rho_*/\rho = 1$ and $L/h = 0$ (see Ref. [18] and references therein). Interestingly the relation between h_*/h and Fr is not affected by the jump type. However, there exists a noticeable gap between the prediction of the Bélanger

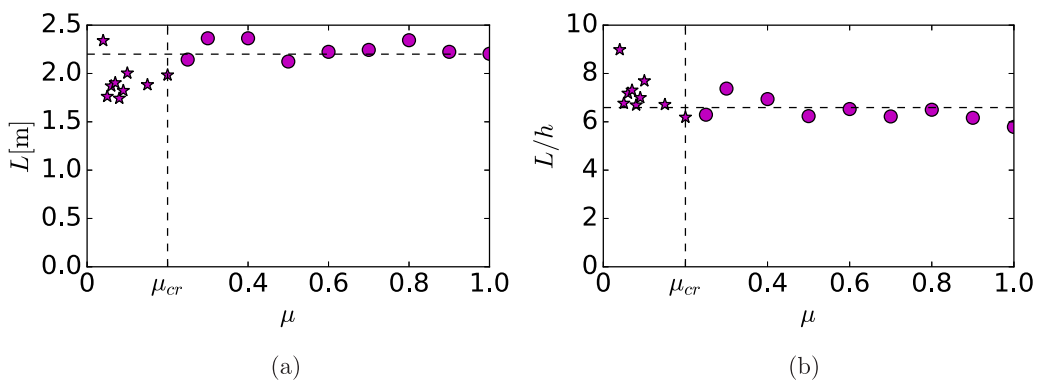


FIG. 13. (a) Jump length L and (b) jump length relative to incoming flow thickness L/h , both against the interparticle friction coefficient μ . The circles represent laminar granular jumps and the stars denote hydraulic-like jumps with a waterlike roller.

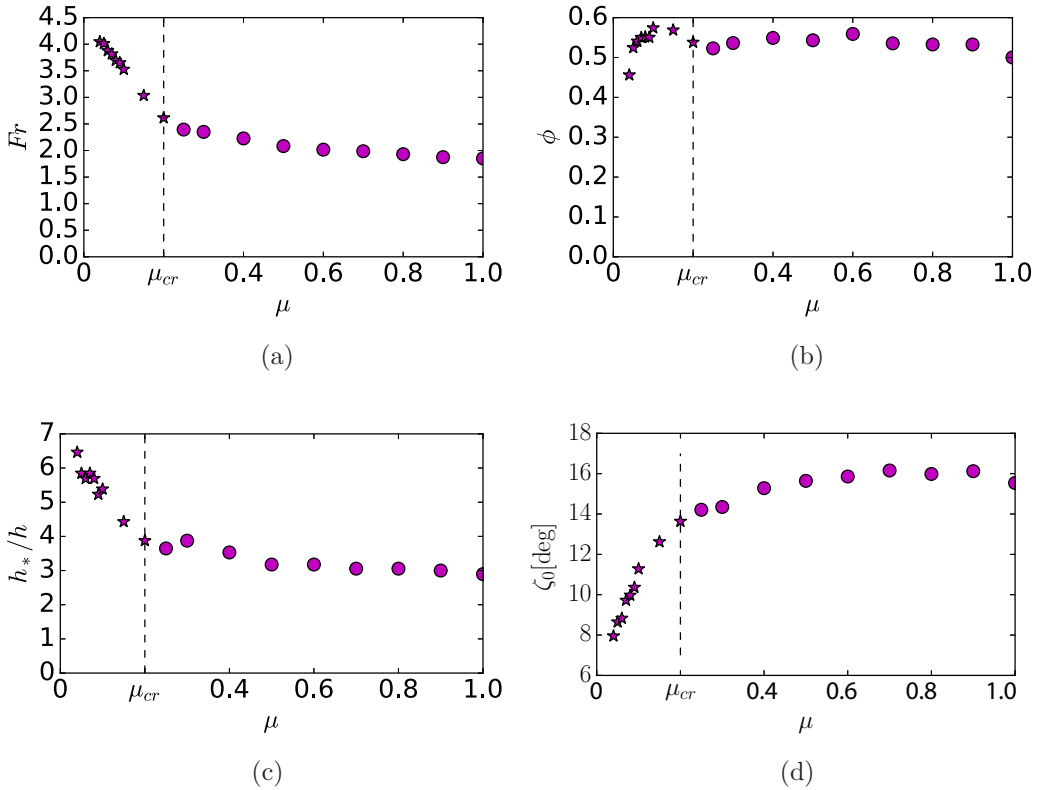


FIG. 14. The transition from laminar granular jumps to hydraulic-like jumps, as visible in Fig. 4, seen through the change in different variables as a function of μ : (a) the Froude number Fr , (b) the incoming volume fraction ϕ , (c) the relative height of the jump h_*/h , and (d) the angle of the free surface after the jump ζ_0 . Stars represent hydraulic-like jumps and dots denote laminar jumps.

equation and the numerical data, which is always above the B elanger model for Fr in the range 1.5–4 and tends to be closer to B elanger equation at higher Froude numbers (range 4–5 in this study). This trend is highlighted by the inset of Fig. 15. This result is in full agreement with previous

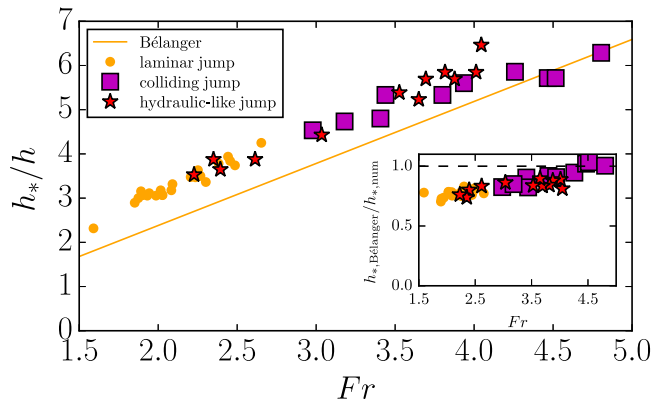


FIG. 15. Jump height ratio, h_*/h , as a function of the Froude number, Fr , for all jumps investigated in the present study. The continuous line shows the prediction of the B elanger equation used in hydraulics (see text).

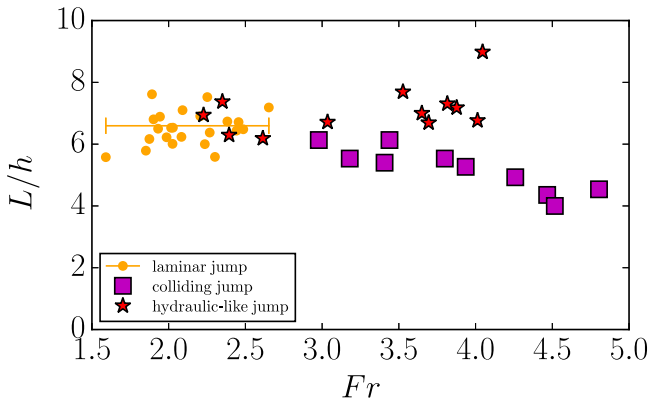


FIG. 16. Dimensionless length of the jump L/h versus the Froude number Fr for all jumps. The orange-colored line shows that L/h is rather constant (within the uncertainty for measuring the jump length) for laminar granular jumps.

experimental results (see Fig. 6 in Ref. [18]) and further highlights the need of a richer theoretical framework for predicting the jump height, for instance based on Eq. (1). In the following we discuss the main outcomes of the present study in terms of the jump length depending on the jump type considered.

B. Length of the jumps

Figure 16 shows the dimensionless length L/h of all the jumps investigated in this study as a function of the Froude number Fr of the incoming flow, by distinguishing the three types of jump identified. One can notice that the relation between L/h and Fr depends on the jump type, which is in strong contrast to the previous results that the relation between h_*/h and Fr is not affected by the jump type (see Fig. 15). Based on Eq. (1), this means that changes in μ_e or ϕ_*/ϕ , are expected to be balanced by a change in L/h , keeping the jump height ratio h_*/h versus Fr constant. This result strongly supports the idea that the length of the jump (L/h) and the constitutive law (μ_e and ϕ_*/ϕ) are interrelated. In other words, the variation of the jump length with Fr and the dissipation mechanisms inside the jump are closely related. Analyzing the differences in terms of the jump length between the various types of jump may give insights into the different dissipation mechanisms inside the jump.

The laminar jump occurs for Fr in the range 1.5–2.5 and its size shows some variability with Fr in that range: The mean value of L/h is around 6.5. The colliding jumps with a recirculation at their foot appear at higher slopes, which correspond to higher Fr . Instead of being constant, L/h is a decreasing function of Fr , ranging from $L/h = 6$ for $Fr = 3$ to $L/h = 4$ for $Fr = 5$. For the jumps with an internal waterlike roller, L/h exhibits a slight increase with Fr . This behavior resembles the increase of L/h with Fr as generally observed with water flows.

It is worthy to note that at a given Froude number, L/h is higher for the hydraulic-like jumps with an internal waterlike roller than for the steep colliding jumps with recirculation taking place close to the free surface at the foot the jump (see for instance the data for $Fr = 4$).

C. Effective friction depending on the jump type

The general framework proposed by Ref. [18] [see Eq. (1) given in the Introduction] can be used to get the effective friction coefficient μ_e inside the jump for the different types of jumps identified

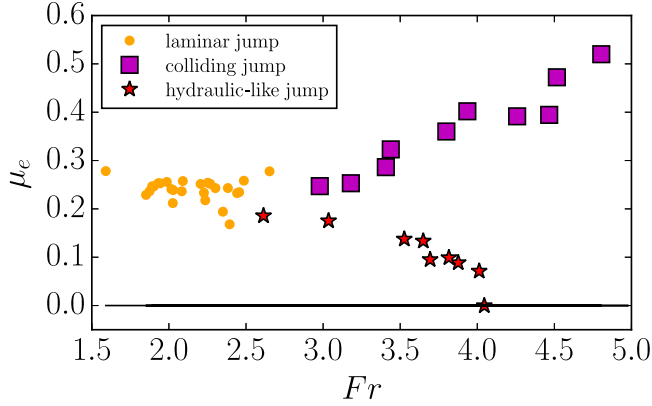


FIG. 17. Effective friction inside the jump μ_e extracted from Eq. (10) as a function of the Froude number for all types of jumps.

in the present work. An expression for μ_e then reads as follows:

$$\mu_e = \tan \zeta + \frac{2Fr^2 \left(\beta - \frac{\beta_*}{\rho} \frac{\rho_* h_*}{h} \right) - k_* \frac{\rho_*}{\rho} \left(\frac{h_*}{h} \right)^2 + k}{K_0 \frac{L}{h} \left(1 + \frac{\rho_* h_*}{\rho h} \right)}, \quad (10)$$

with K_0 a shape factor so that the weight per unit width of the jump can be written as $w = K_0 g L (\rho h + \rho_* h_*) / 2$, as initially introduced by [15]:

$$K_0 = \frac{2 \int_0^L \rho(x) h(x) dx}{L(\rho h + \rho_* h_*)}, \quad (11)$$

where $\rho(x)$ and $h(x)$ are the density and height (respectively) of the flow inside the jump. The earth pressure coefficients k and k_* before and after the jump are both taken equal to 1 in this study (for further discussion see Refs. [17,18,33]). The Boussinesq momentum coefficients β and β_* , which correspond to the ratios between the depth-averaged value of the velocity-squared and the square of the depth-averaged velocity (see also introduction), are directly extracted from the DEM simulations (from the velocity profiles shown in Figs. 5, 7, and 9). The effective friction coefficient μ_e is a good indicator of the efficiency of energy dissipation inside the jump for each type of jump. The variation of μ_e with Fr is plotted for all our jumps in Fig. 17. One observes a remarkable difference between the types of jump: μ_e is independent of Fr for the laminar granular jumps but is an increasing function of Fr for the steep colliding granular jumps, and even becomes a decreasing function of Fr for the hydraulic-like jumps. Note that the general relation established under the assumption of a Coulomb rheology and proposed for granular jumps by Méjean *et al.* [18] may be questionable when the interparticle friction coefficient μ is lower than μ_{cr} . As such, the value μ_e extracted from Eq. (10) should be considered with caution in the case of hydraulic-like jumps with a roller. This is, however, a useful way to further highlight the differences between the latter jump type and the other jumps.

Figure 17 and the general behavior of the jumps (streamlines patterns, recirculation or not, evolution of the length with input parameters) can help in drawing some underlying assumptions for the development of a dissipation model depending on the jump type. More generally, this may provide crucial insights on the physics of flowing granular matter.

The effective friction inside the jumps, μ_e , and the length of the jumps relative to the incoming flow thickness, L/h , are constant with the Froude number in case of laminar granular jumps [circles in Fig. 10(a) and 17]. The jump length is sensitive to changing the thickness of the flow: Increasing either the mass discharge (through H) or the grain diameter (d) produces an increase of the jump

length, but the ratio L/h remains independent of either H or d . The streamlines show a gradual transition from the stable state upstream from the jump to the stable state after the jump, and the granular flow is dense. All of this suggests that the dominant dissipation process for this type of jumps stems from enduring frictional contacts between the grains.

As the recirculation inside the jump increases, the length L of the jump decreases [squares in Fig. 10(a)], while the effective friction μ_e within the jump increases (squares in Fig. 17). This highlights the dissipative role of the recirculation phenomenon. In those types of jumps, there are still enduring frictional contacts between the grains, but binary gaseouslike collisions come into play in the recirculation zone (evidenced by the overall shapes of the streamlines and the drop in the depth-averaged volume fraction along the chute). This observation indicates that the steep jump, with a granular recirculation zone, is efficient at dissipating energy over a shorter distance. The presence of the recirculation zone characterized by active bouncing of particles probably contributes to higher rates of energy dissipation. This suggests that a theory describing energy dissipation in granular jumps at high ζ (high Fr) should not be limited to including a frictional term only but should also account for a collisional term. For such jumps with fast and thin incoming flows, μ_e may be written (in first approximation) as the sum of a constant Coulombian friction μ_s and a velocity-squared dependent term in the form αFr^2 . Note that, however, we could not find any relevant values of μ_s and α to fit at the same time both the laminar (circles in Fig. 15) and the colliding (squares in Fig. 17) granular jump data, in contrast to the analysis proposed earlier by Méjean *et al.* [18], applied to jumps measured in the laboratory [16]. This result motivates future work.

Figure 17 shows that as the friction between the grains decreases (stars shown on the plot), the effective friction inside the jump μ_e decreases as well. This is because as μ decreases, the enduring frictional contacts between the grains are less efficient at dissipating energy and a waterlike roller can form. There is a large drop in volume fraction across most of the jump, indicating a very loose grain packing inside that roller. Figure 17 shows that μ_e , extracted from Eq. (10), may even reach zero for $\mu = 0.04$. Note that the incoming flows produced by simulations with μ below 0.04 (not shown here) were so gaseous that it was impossible to measure the depth-averaged variables properly. For the hydraulic-like jumps, because of the presence of that roller, it will certainly be relevant to infer a general jump height relation relying on a turbulent-like effective shear stress (similar to the one proposed for instance in Ref. [18] for water flows), instead of the Coulombian shear stress which was deemed necessary for the derivation of Eq. (10). The transition from a steep colliding granular jump to a hydraulic-like jump with a roller is caused by the lowering of interparticle friction. This process of the transformation of the granular recirculation at the foot of the jump into a fully developed roller inside the jump warrants further investigation.

VI. SUMMARY AND CONCLUSION

The discrete numerical simulations carried out in the present study have revealed the existence of three types of granular jumps that show different geometries and internal dynamics and therefore emphasise different regimes of the constitutive friction law—in terms of the effective friction coefficient μ_e as a function of the Froude number Fr of the incoming flow (under a depth-averaged framework). At low Fr , laminar granular jumps were characterized by slowly varying streamlines and a monotonic and gradual increase of the density along the jump. The resulting effective friction μ_e was nearly constant regardless of the Froude number of the incoming flow. For higher Fr , steep colliding jumps occurred with sharp variation of the streamlines and the formation of a recirculation close to the free surface, accompanied by a drop in density. The effective friction μ_e was found to increase with the Froude number of the incoming flow. The latter two types of jump were obtained for a typical interparticle friction of about 0.5. When decreasing the interparticle friction below a critical value (0.2 in the numerical simulations done here), the laminar granular jump turned into a hydraulic-like jump with the formation of an internal roller which extended over the whole length of the jump, and a well-identified (sharp) drop in density occurred. In this case, μ_e was shown to be a decreasing function of the Froude number of the incoming flow. The present study demonstrates

that the standing granular jump may be seen as a stringent test for the dominant term controlling the constitutive form of the friction law as affected by its interrelation with the internal dynamics of the granular medium. Therefore, the granular jump can be seen as a useful gauge for addressing the dissipation mechanisms that govern the flowability of granular media, in addition to the other flow configurations traditionally used to investigate the rheology of granular flows, such as plane shear flows [19], annular shear cell flows [34] or steady and uniform flows down inclines [35].

ACKNOWLEDGMENTS

The authors are thankful to the Labex Tec21, which is part of the ANR “Investissements d’avenir” program for funding. S.M. is grateful to the funds provided by both the IDEX Graduate School of University of Grenoble Alpes (ANR “Investissements d’avenir” program) and the Region Auvergne-Rhône-Alpes (ExploRa Doc scholarship scheme). T.F. thanks additional funding by French ministries “Ministère de l’Europe et des Affaires Etrangères” and “Ministère de l’Enseignement Supérieur, de la Recherche et de l’Innovation” in the frame of the PHC project GrainFlow within the FASIC 2017 program.

APPENDIX A: DISCUSSION ON THE COARSE-GRAINING TECHNIQUE

This Appendix discusses the coarse-graining technique used and the choices made for the present study, specifically dedicated to the macroscopic features of standing jumps formed during granular flows down inclines. The reader can refer to Refs. [24,25,36–39], and a number of references therein, for detailed descriptions of the existing coarse-graining techniques, including very refined methods.

A series of simulations was carried out for one jump type, considering one given set of input conditions ($H = 0.5$ m, $\zeta = 25^\circ$) and the default values given in Table I for the micro parameters d , μ , μ_b , and e , and by systematically varying the range c of the Lucy function from $c/d = 0.75$ to $c/d = 10$. It was found that the results in terms of jump geometry (ratios L/h and h_*/h) were independent of c/d as long as c/d was kept below $h/2$ ($h \sim 9d$ for the set of parameters considered for the corresponding series of simulations). However a slight influence of c on the measured volume fractions was detected. Figure 18 shows the depth-averaged values of the volume fractions ϕ and ϕ_* as a function of c/d .

The volume fraction after the jump is nearly constant and independent of c/d over a narrow range of c/d , which typically ranges from 2 to 4.5 for the jump type investigated here. The lower limit (see the vertical continuous line drawn on Fig. 18) is fully consistent with the conclusions of previous works showing that values of the coarse-graining width, $w = c/2$, below the grain diameter should be avoided, as early reported by previous studies on 2D shear-cell flows [37] and 3D granular flows [25]. Very small values of the coarse-graining width ($w < 0.1d$) could have been considered to capture the oscillations of volume fraction but this would have required data acquisition at very high frequency, as investigated in details by Weinhart *et al.* [25] (see also the discussion at the end of the present Appendix). The upper limit of c/d (~ 4.5 , as indicated by the vertical dashed line drawn on Fig. 18) above which ϕ_* starts to decrease significantly with c/d is also consistent with previous studies showing that too large values of the coarse-graining width (close to the system size) should be avoided [25,37] because of side-effects close to boundaries. The latter effects are even more pronounced in the case of the shallow and stratified incoming flows (that take place before the jump) because the two boundaries, namely the bottom and the free surface of the flow, become very close. This explains why the volume fraction ϕ of the incoming flows is sensitive to c/d . Figure 18 shows that ϕ slightly varies even when c is in the range $[2d, 4.5d]$, as materialized by the two vertical lines drawn in Fig. 18. However the variation of ϕ in that range of c is less than 5-10% and does not affect the main results of the present study in terms of the effective friction μ_e as a function of the Froude number Fr (see Fig. 17). It is clear from Fig. 18 that above a critical c/d —of about $h/2$ —the volume fraction drastically drops because of the combined effects caused by the bottom and the free surface boundaries, thus causing a large underestimate of the volume

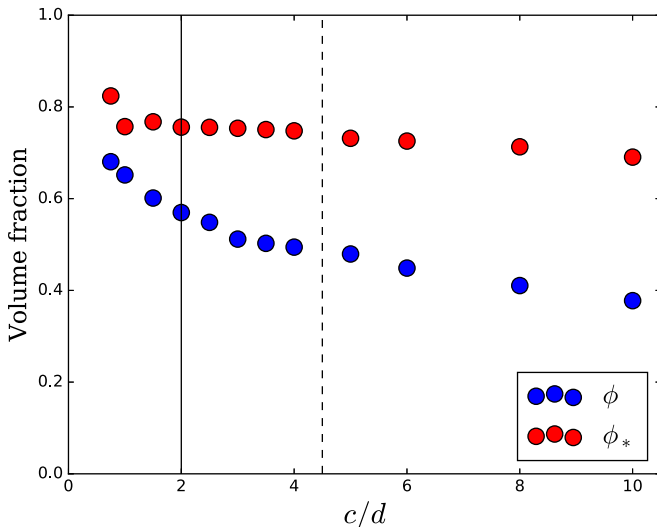


FIG. 18. Volume fractions measured before (ϕ) and after (ϕ_*) the jump as a function of the range c of the Lucy function scaled by the grain diameter (c/d). Simulations done for $H = 0.5$ m and $\zeta = 25^\circ$, considering the default values given in Table I for d , μ , μ_b , and e .

fraction. Moreover, it should be noted here that the data shown in Fig. 18 do not correspond to the thinnest flows investigated in the present study. For the thinnest flows ($h/d \sim 6$), the upper limit of c should be $h/2 \sim 3d$. Considering both that upper limit given by the thickness of the thinnest flows and the lower limit of $c \sim 2d$ ($w \sim d$), one can conclude that $c = 2.5d$ was a very good compromise for the present study.

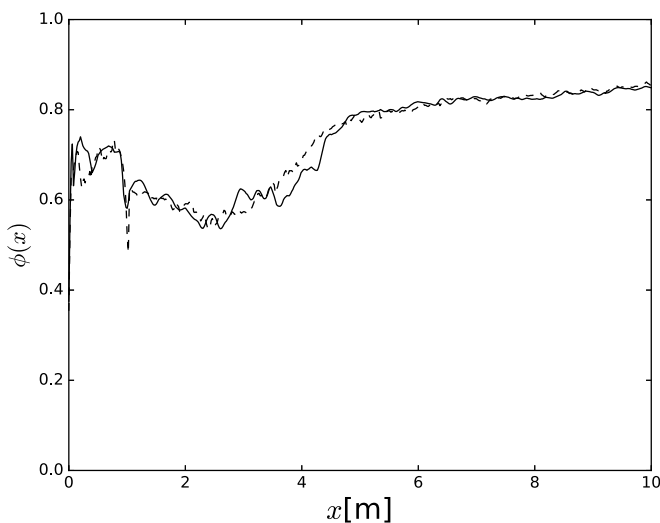


FIG. 19. Evolution of the depth-averaged volume fraction along the chute: comparison between time-averaged results sampling data every 0.3 s (continuous line) or 1 s (dashed line). Simulations done for $H = 0.5$ m and $\zeta = 25^\circ$, considering the default values given in Table I for d , μ , μ_b , and e , and taking $c = 2.5d$ for the range of the Lucy function.

In order to analyze in detail how a number of micro- and macroparameters influence the granular jump patterns, the computational costs were drastically reduced by registering only a small fraction of the data over time. As explained in the main text, the average in time was a direct average of the instantaneous coarse-grained fields extracted every 1000 time step (0.3 s), and the instantaneous fields were chosen separated enough in time to ensure minimum correlation between the individual grain positions at successive coarse-grained time steps. Figure 19 shows the evolution of the depth-averaged volume fraction along the chute measured with this method (as used for the present study) and it is compared to another signal obtained by using an even more degraded acquisition rate (every 1 s). It can be concluded from the two curves that the choice made for time-averaging was largely sufficient (on the safe side) to get robust measurements of the steady-state quantities, such as the depth-averaged volume fraction along the chute.

Investigations on the fluctuating behavior of the granular flows and jumps would demand refinement on the coarse-graining technique, by considering very small values of the coarse-graining width combined with much longer simulations at steady state (still avoiding issues related to the existence of correlations between individual grain positions at successive coarse-grained time steps) for consistent time-averaging or ensemble averaging [25]. Refined coarse-graining by taking into account the gradients within the averaging region properly was developed recently and also offers a robust method for meaningful measurements of the fluctuating behavior of shallow granular flows [36]. Capturing the oscillations of the granular flow and jumps due to layering was beyond the scope of the present study.

-
- [1] Y. Forterre and O. Pouliquen, Flows of dense granular media, *Annu. Rev. Fluid Mech.* **40**, (2007).
 - [2] H. M. Jaeger, S. R. Nagel, and R. P. Behringer, Granular solids, liquids, and gases, *Rev. Mod. Phys.* **68**, 1259 (1996).
 - [3] GDR Midi, On dense granular flows, *Eur. Phys. J. E* **14**, 341 (2004).
 - [4] J. Boudet, Y. Amarouchene, B. Bonnier, and H. Kellay, The granular jump, *J. Fluid Mech.* **572**, 413 (2007).
 - [5] C. G. Johnson and J. M. N. T. Gray, Granular jets and hydraulic jumps on an inclined plane, *J. Fluid Mech.* **675**, 87 (2011).
 - [6] T. Faug, Depth-averaged analytic solutions for free-surface granular flows impacting rigid walls down inclines, *Phys. Rev. E* **92**, 062310 (2015).
 - [7] S. P. Pudasaini and C. Kröner, Shock waves in rapid flows of dense granular materials: Theoretical predictions and experimental results, *Phys. Rev. E* **78**, 041308 (2008).
 - [8] S. Viroulet, J. L. Baker, A. N. Edwards, C. G. Johnson, C. Gjaltema, P. Clavel, and J. M. N. T. Gray, Multiple solutions for granular flow over a smooth two-dimensional bump, *J. Fluid Mech.* **815**, 77 (2017).
 - [9] C. Brennen, K. Sieck, and J. Paslaski, Hydraulic jumps in granular material flow, *Powder Technol.* **35**, 31 (1983).
 - [10] C. Campbell, C. Brennen, and R. Sabersky, Flow regimes in inclined open-channel flows of granular materials, *Powder Technol.* **41**, 77 (1985).
 - [11] H. Morrison and O. Richmond, Application of spencer's ideal soil model to granular materials flow, *J. Appl. Mech.* **43**, 49 (1976).
 - [12] H. Xiao, J. Hruska, J. M. Ottino, R. M. Lueptow, and P. B. Umbanhowar, Unsteady flows and inhomogeneous packing in damp granular heap flows, *Phys. Rev. E* **98**, 032906 (2018).
 - [13] Y.-C. Tai, and Y.-C. Lin, A focused view of the behavior of granular flows down a confined inclined chute into the horizontal run-out zone, *Phys. Fluids* **20**, 123302 (2008).
 - [14] J. M. N. T. Gray, Y.-C. Tai, and S. Noelle, Shock waves, dead zones and particle-free regions in rapid granular free-surface flows, *J. Fluid Mech.* **491**, 161 (2003).
 - [15] S. B. Savage, Gravity flow of cohesionless granular materials in chutes and channels, *J. Fluid Mech.* **92**, 53 (1979).

- [16] T. Faug, P. Childs, E. Wyburn, and I. Einav, Standing jumps in shallow granular flows down smooth inclines, *Phys. Fluids* **27**, 073304 (2015).
- [17] T. Faug, Jumps and bores in bulky frictional granular flows, in *Powders and Grains 2013: Proceedings of the 7th International Conference on Micromechanics of Granular Media*, Vol. 1542 (AIP Publishing, Sydney, 2013), pp. 642–645.
- [18] S. Méjean, T. Faug, and I. Einav, A general relation for standing normal jumps in both hydraulic and dry granular flows, *J. Fluid Mech.* **816**, 331 (2017).
- [19] F. da Cruz, S. Emam, M. Prochnow, J.-N. Roux, and F. Chevoir, Rheophysics of dense granular materials: Discrete simulation of plane shear flows, *Phys. Rev. E* **72**, 021309 (2005).
- [20] P. Jop, Y. Forterre, and O. Pouliquen, A constitutive law for dense granular flows, *Nature* **441**, 727 (2006).
- [21] V. Smilauer, A. Gladky, J. Kozicki, C. Modenese, and J. Stronsky, Yade, using and programming, in *Yade Documentation*, 1st ed. edited by V. Smilauer (The Yade Project, Prague, 2010).
- [22] S. Méjean, T. Faug, and I. Einav, Discrete element method simulations of standing jumps in granular flows down inclines, in *EPJ Web of Conferences*, Vol. 140 (EDP Sciences, 2017), p. 03026.
- [23] C. Goldenberg and I. Goldhirsch, *Continuum Mechanics for Small Systems and Fine Resolutions* (American Scientific, Stevenson Ranch, CA, 2006).
- [24] I. Goldhirsch, Stress, stress asymmetry and couple stress: From discrete particles to continuous fields, *Granul. Matter* **12**, 239 (2010).
- [25] T. Weinhart, R. Hartkamp, A. R. Thornton, and S. Luding, Coarse-grained local and objective continuum description of three-dimensional granular flows down an inclined surface, *Phys. Fluids* **25**, 070605 (2013).
- [26] L. B. Lucy, A numerical approach to the testing of the fission hypothesis, *Astron. J.* **82**, 1013 (1977).
- [27] W. G. Hoover and C. G. Hoover, Smooth-particle phase stability with generalized density-dependent potentials, *Phys. Rev. E* **73**, 016702 (2006).
- [28] P. Rognon, T. Miller, and I. Einav, A circulation-based method for detecting vortices in granular materials, *Granul. Matter* **17**, 177 (2015).
- [29] A. Savitzky and M. J. Golay, Smoothing and differentiation of data by simplified least squares procedures, *Anal. Chem.* **36**, 1627 (1964).
- [30] J. M. N. T. Gray and X. Cui, Weak, strong and detached oblique shocks in gravity-driven granular free-surface flows, *J. Fluid Mech.* **579**, 113 (2007).
- [31] N. Brodu, P. Richard, and R. Delannay, Shallow granular flows down flat frictional channels: Steady flows and longitudinal vortices, *Phys. Rev. E* **87**, 022202 (2013).
- [32] H. Chanson, Development of the bélanger equation and backwater equation by Jean-Baptiste Bélanger (1828), *J. Hydraul. Eng.* **135**, 159 (2009).
- [33] S. B. Savage and K. Hutter, The motion of a finite mass of granular material down a rough incline, *J. Fluid Mech.* **199**, 177 (1989).
- [34] A. Fall, G. Ovarlez, D. Hautemayou, C. Mézière, J.-N. Roux, and F. Chevoir, Dry granular flows: Rheological measurements of the $\mu(i)$ -rheology, *J. Rheol.* **59**, 1065 (2015).
- [35] O. Pouliquen, Scaling laws in granular flows down rough inclined planes, *Phys. Fluids* **11**, 542 (1999).
- [36] R. Artoni and P. Richard, Average balance equations, scale dependence, and energy cascade for granular materials, *Phys. Rev. E* **91**, 032202 (2015).
- [37] M. Lätzel, S. Luding, and H. J. Herrmann, Macroscopic material properties from quasi-static, microscopic simulations of a two-dimensional shear-cell, *Granul. Matter* **2**, 123 (2000).
- [38] A. Thornton, T. Weinhart, V. Ogarko, and S. Luding, Multi-scale methods for multi-component granular materials, *Comput. Methods Mater. Sci.* **13**, 197 (2013).
- [39] T. Weinhart, A. R. Thornton, S. Luding, and O. Bokhove, From discrete particles to continuum fields near a boundary, *Granul. Matter* **14**, 289 (2012).